Acta Mech 223, 309–330 (2012)
DOI 10.1007/s00707-011-0563-2

B. Sobhani Aragh · H. Hedayati

Static response and free vibration of two-dimensional functionally graded metal/ceramic open cylindrical shells under various boundary conditions

Received: 11 May 2011 / Published online: 30 October 2011

Abstract The free vibration and static response of a two-dimensional functionally graded (2-D FGM) metal/ceramic open cylindrical shell are analyzed using 2-D generalized differential quadrature method. The open cylindrical shell is assumed to be simply supported at one pair of opposite edges and arbitrary boundary conditions at the other edges such that trigonometric functions expansion can be used to satisfy the boundary conditions precisely at simply supported edges. This paper presents a novel 2-D power-law distribution for ceramic volume fraction of 2-D FGM that gives designers a powerful tool for flexible designing of structures under multifunctional requirements. Various material profiles in two radial and axial directions are illustrated using the 2-D power-law distribution. The effective material properties at a point are determined in terms of the local volume fractions and the material properties by the Mori–Tanaka scheme. The 2-D generalized differential quadrature method as an efficient and accurate numerical tool is used to discretize the governing equations and to implement the boundary conditions. The convergence of the method is demonstrated, and to validate the results, comparisons are made with the available solutions for FGM cylindrical shells. The interesting results indicate that a graded ceramic volume fraction in two directions has a higher capability to reduce the mechanical stresses and natural frequency than conventional 1-D FGM. The achieved results confirm that natural frequency and mechanical stress distribution can be modified to a required manner by selecting an appropriate volume fraction profile in two directions.

1 Introduction

Functionally graded materials (FGMs) are materials, in which the volume fraction of two or more materials is varied continuously as a function of the position along certain dimension(s) from one point to another. The FGMs are usually made of a ceramic/metal mixture with an arbitrary composition of each one, and the volume fraction of each material is changed gradually. By gradually varying the volume fraction of constituent materials, their material properties exhibit a smooth and continuous change from one surface to another, thus eliminating interface problems and mitigating thermal stress concentrations. This is due to the fact that the ceramic constituents of FGMs are able to withstand high-temperature environments due to their better thermal resistance characteristics, while the metal constituents provide stronger mechanical performance and reduce the possibility of catastrophic fracture.

B. Sobhani Aragh (✉)
Department of Mechanical Engineering, Arak Branch, Islamic Azad University, Arak, Iran
E-mail: behnamsobhani@yahoo.com
Tel.: +98 9364978879
Fax: +98 8314274542

H. Hedayati
Department of Mechanical Engineering, Aligudarz Branch, Islamic Azad University, Aligudarz, Iran

Some research papers on the analysis of functionally graded structures are available. Woo and Meguid [1] gave an analytical solution for the large deflection of thin FG plates and shallow shells under transverse loading and temperature field. Based on the von Karman theory for large transverse deflection, the fundamental equations for shallow thin rectangular FG shells have been presented. Loy et al. [2] and Pradhan et al. [3] have studied the vibration of functionally graded cylindrical shells using Love's shell theory and the Rayleigh–Ritz method. The free vibration problem of simply supported rectangular plates with general inhomogeneous material properties along the thickness direction was analyzed by Chen et al. [4]. Huang and Shen [5] dealt with the nonlinear vibration and dynamic response of a functionally graded material plate with surface-bonded piezoelectric layers in thermal environments. Sobhani Aragh and Yas [6] studied the 3-D free vibration of functionally graded fiber orientation and volume fraction of cylindrical panels. The interesting and new results show that the normalized natural frequency of the functionally graded fiber orientation cylindrical panel is smaller than that of a discrete laminate composite panel and close to that of a 4-layer. In contrast, the normalized natural frequency of a functionally graded fiber volume fraction is larger than that of a discrete laminated and close to that of a 2-layer. Zhao et al. [7] investigated the static response and free vibration of FGM shells subjected to mechanical or thermomechanical loading using the element-free kp-Ritz method. Sander's first-order shear deformation shell theory was employed to develop the transverse shear strain–stress relation. Sobhani Aragh and Yas [8] investigated the effect of symmetric and asymmetric volume fraction profiles on the static and free vibration characteristics of continuously graded fiber-reinforced (CGFR) cylindrical shells with a generalized power-law distribution, And very recently, these authors [9] studied the effect of continuously grading fiber orientation face sheets on the free vibration of sandwich panels with functionally graded core. The face sheets had a variation of the fiber orientation, while the core had a variation of the fiber volume fraction.

In the above-mentioned papers, the material properties are assumed having a smooth variation usually in one direction. In 2003, the Columbia space shuttle was lost in a catastrophic breakup due to outer surface insulation that fell loose when the Columbia lifted off. The physical cause of the loss of Columbia and its crew was a breach in the thermal protection system on the leading edge of the left wing, caused by a piece of insulating foam, which separated from the left bipod ramp section of the external tank and struck the wing in the vicinity of the lower half of a reinforced carbon–carbon panel. During reentry, this breach in the thermal protection system allowed superheated air to penetrate through the leading edge insulation and progressively melt the aluminum structure of the left wing, resulting in a weakening of the structure until increasing aerodynamic forces caused loss of control, failure of the wing and breakup of the Orbiter [10,11]. Such damage to the space shuttle's protective thermal tiles can be prevented by using FGMs. It is worth mentioning that a conventional functionally graded material may also not be so effective in such design problems since all outer surfaces of the body will have the same composition distribution and temperature distribution in such advanced machine element changes in two or three directions. Therefore, if the FGM has 2-D dependent material properties, a more effective high-temperature-resistant material can be obtained. Based on this fact, 2-D functionally graded materials (2-D FGMs) whose material properties are bidirectionally dependent are introduced. The manufacturing of multidimensional FGM may seem to be costly or difficult, but it should be noted that while these technologies are relatively new, processes such as 3-D printing (3-DP^{TM}) and laser engineering net shaping (LENS$^{(R)}$) can currently produce FGMs with relatively arbitrary three-dimensional grading [12]. With further refinements, FGM manufacturing methods may provide the designers with more control of the composition profile of functionally graded components with reasonable costs.

Recently, many investigations for 2-D FGM have been carried out. The thermal stresses in two-directionally graded aerospace shuttles and crafts were later studied by Nemat–Alla [13] using a finite element model. The same technique was later applied by Hedia [14] for the stress analysis on the backing shell of the cemented acetabular cup made of FGMs. He found that some critical stresses of concern for shells fabricated by unidirectional or 2-D FGMs were reduced by more than 50% compared with shells made of homogeneous materials. A further reduction of stresses was achieved using 2-D FGMs rather than unidirectional FGMs when designing cementless hip stems [15]. Sutradhar and Paulino [16] used the boundary element method to investigate the heat conduction problems of 2-D FGMs, while the Green's functions were obtained by Chan et al. [17] for 2-D unbounded spaces with the shear modulus varying in two directions. Qian and Batra [18] made use of the meshless local Petrov–Galerkin (MLPG) method to obtain numerical solutions for static, free, and forced vibrations of a cantilever beam, for which material properties are power-law functions of the two coordinates. Asgari et al. [19] studied the dynamic behavior of a 2-D FG thick hollow cylinder with finite length under impact loading, and also Asgari and Akhlaghi [20] investigated the transient thermal stresses in a 2-D FGM thick hollow cylinder with finite length by using the finite element method with graded material properties within each element. Nemat–Alla et al. [21] studied the elastic–plastic analysis of 2-D functionally graded materials under thermal loading. They showed that heat conductivity of the metallic constituents of FGM has a

large effect on the temperature distribution that resulted from the thermal loads. Kutiš et al. [22] presented the multilayering method and the direct integration method for modeling of a functionally graded material (FGM) beam with continuous spatially varying material properties. Goupee and Vel [23] proposed a methodology for the 2-D simulation and optimization of the material composition distribution of an FGM. The 2-D quasi-static heat conduction and thermo-elastic problems were analyzed using the element-free Galerkin method. Ke and Wang [24] developed a multilayered model for frictionless contact analysis of functionally graded materials (FGMs) with arbitrarily varying elastic modulus under plane strain-state deformation. The FGM was divided into several sublayers, and in each sublayer, the shear modulus was assumed to be a linear function while the Poisson's ratio was assumed to be a constant. With the model, the frictionless contact problem of a functionally graded coated half-space was investigated.

Some researchers [8,25–28] have studied the influence of the power-law exponent, of the power-law distribution choice, and of the choice of the different parameters on the free vibrations of conventional functionally graded shells and panels. Moreover, analyses available in these papers are based on the assumption that the material properties have a specific variation in one direction. As mentioned above, a conventional FGM may also not be so effective in such design problems since all outer surfaces of the body will have the same composition distribution. This paper presents a novel 2-D power-law distribution for the ceramic volume fraction of a 2-D FGM that gives designers a powerful tool for flexible designing of structures under multifunctional requirements. Various material profiles in two radial and axial directions can be illustrated using a 2-D six-parameter power-law distribution. In fact, using a 2-D power-law distribution, it is possible to study the influence of the different kinds of two-directional material profiles including symmetric and classical ones on the natural frequencies and mechanical stress components of a shell. Furthermore, the maximum stresses and stress distribution can be modified to a required manner by selecting suitable different parameters of a power-law distribution and volume fraction profiles in two directions. To the best knowledge of the authors, there is no analysis available in the open literature for the free vibration and static response of 2-D functionally graded metal/ceramic open cylindrical shells under various boundary conditions. In this study, a graded open cylindrical shell with 2-D power-law distribution of the volume fraction of the constituents in two radial and axial directions is considered. The Mori–Tanaka scheme as an accurate micromechanics model is used for estimating the homogenized material properties. The 2-D generalized differential quadrature method (GDQM) is efficiently used to discretize the governing equations and to implement the related boundary conditions. The effects of different boundary conditions, various geometrical parameters and different ceramic volume fraction profiles in radial and axial directions on the vibration and static behavior of 2-D FGM metal/ceramic open cylindrical shells are investigated.

2 Problem formulation

Let us consider a 2-D FGM open cylindrical shell of length L_x, mean radius Z_m, uniform thickness h, as shown in Fig. 1. An orthogonal cylindrical coordinate system (x, θ, z) is used to label the material point of the plate in the unstressed reference configuration.

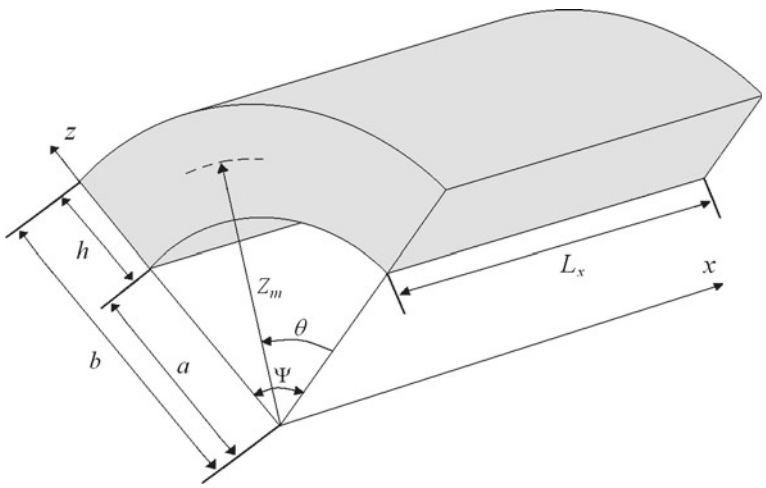

Fig. 1 Geometry of 2-D FGM open cylindrical shell

Table 1 Material properties of aluminum and silicon carbide

	Young's modulus, E (GPa)	Poisson's ratio, v	Mass density, ρ (Kg/m^3)
Al	70	0.30	2,707
Silicon carbide (SiC)	410	0.170	3,100

2.1 2-D FGM constitutive law

In the conventional 1-D FGM shell, the shell's material is graded in one direction. The 1-D FGM shells have a smooth variation of material volume fractions, and/or in-plane fiber orientations, through the radial direction [6–9,25–28]. Significant advances in fabrication and processing techniques have made it possible to produce FGMs using processes that allow FGMs with complex properties and shapes, including 2-and 3-D gradients using computer-aided manufacturing techniques. For the 2-D FGMs, the material properties are continuous functions of the coordinates, and the volume fractions of the constituents vary in a predetermined composition profile. Now consider a two-phase graded material with a power-law variation of the volume fraction of the constituents in the radial and axial directions. The material properties of aluminum and silicon carbide are listed in Table 1 [29,30]. In this paper, it is proposed that the volume fraction of the ceramic phase follows a 2-D six-parameter power-law distribution:

$$2-\text{D FGM}: V_c = \left((V_b - V_a)\left(\left(\frac{1}{2} - \frac{z - Z_m}{z_o - z_i}\right) + \alpha_z \left(\frac{1}{2} + \frac{z - Z_m}{z_o - z_i}\right)^{\beta_z}\right)^{\gamma_z} + V_a\right) \times \left(1 - \left(\frac{x}{L_x}\right) + \alpha_x \left(\frac{x}{L_x}\right)^{\beta_x}\right)^{\gamma_x} \tag{1}$$

where the radial volume fraction index γ_z, and the parameters α_z, β_z and axial volume fraction index γ_x, and the parameters α_x, β_x govern the material variation profile through the radial and axial directions, respectively. The volume fractions V_a and V_b, which have values that range from 0 to 1, denote the ceramic volume fractions of the two different isotropic materials. For example, with the assumption $V_b = 1$ and $V_a = 0.3$, some material profiles in the radial ($\eta_z = (z - Z_m)/h$) and axial ($\eta_x = x/L$) directions are illustrated in Figs. 2, 3 and 4. As can be seen from Fig. 2, the classical volume fraction profiles in the radial and axial directions are presented as special case of the 2-D power-law distribution (1) by setting $\alpha_z = \alpha_x = 0$ and $\gamma_z = \gamma_x = 4$. In Fig. 2, for the first 2-D power-law distribution (1), the ceramic volume fraction decreases through the thickness from 1 at $\eta_z = -0.5$ to 0.3 at $\eta_z = 0.5$. Likewise, the ceramic volume fraction decreases in the axial direction from 1 at $\eta_x = -0.5$ to 0 at $\eta_x = 0.5$. With another choice of the parameters α_z, β_z, α_x and β_x, it is possible to obtain symmetric volume fraction profiles in the radial and axial directions as shown in Fig. 3. Classical and symmetric profiles in the radial and axial directions are obtained by setting $\alpha_z = 0, \alpha_x = 1$

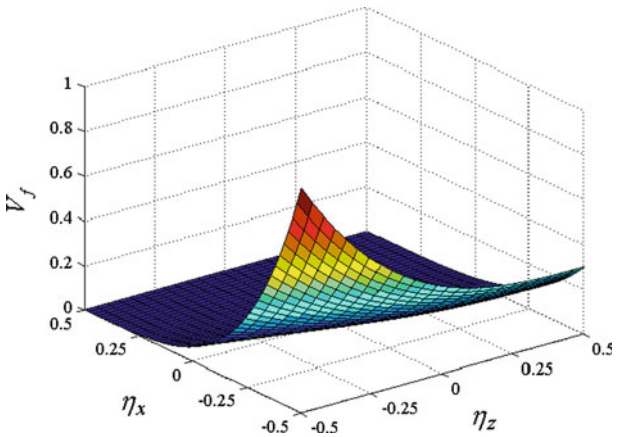

Fig. 2 Variations of the classical volume fraction profile in the radial and axial directions ($\alpha_z = \alpha_x = 0, \gamma_z = \gamma_x = 4$)

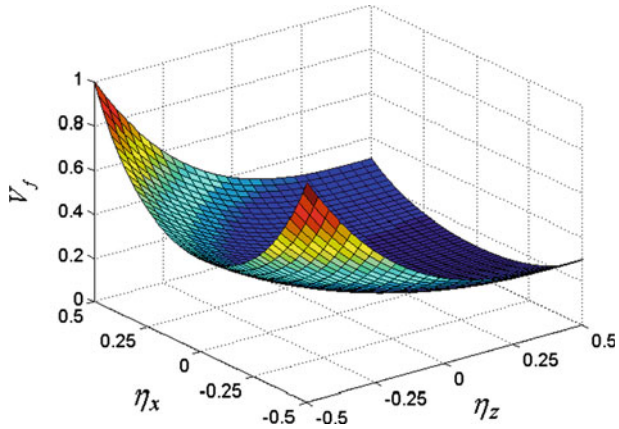

Fig. 3 Variations of the volume fraction profile in the radial and axial directions ($\gamma_z = \gamma_x = 3$)($\alpha_z = 1, \beta_z = 2, \alpha_x = 0$)

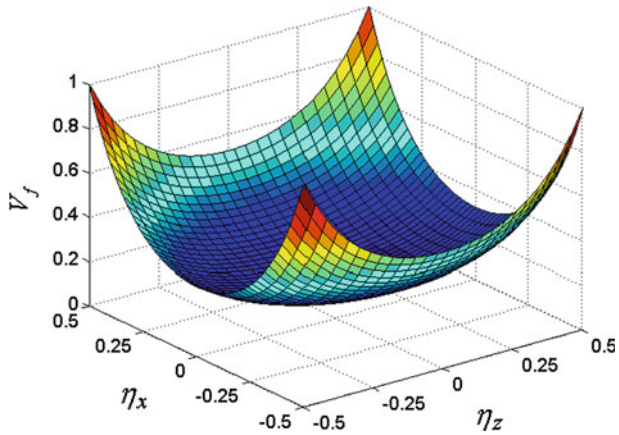

Fig. 4 Variations of the symmetric volume fraction profiles in the radial and axial directions ($\alpha_z = \alpha_x = 1, \beta_z = \beta_x = 2, \gamma_z = \gamma_z = 3$)

and $\beta_x = 2$ in Eq. (1). Figure 3 shows a classical profile versus η_z and a symmetric profile versus η_x. As observed, the ceramic volume fraction on the lower edge ($\eta_x = -0.5$) is the same as that on the upper edge ($\eta_x = 0.5$). Figure 4 illustrates symmetric profiles through the radial and axial directions obtained by setting $\alpha_z = 1, \alpha_x = 1$ and $\beta_z = 2, \beta_x = 2$. Sobhani Aragh and Yas [8,9] and [28] studied the variations of the classical and symmetric profiles of conventional 1-D functionally graded panels with radial volume fraction index.

The effective material properties of the isotropic 2-D FGMs are determined in terms of the local volume fractions and material properties of the two isotropic phases by the Mori–Tanaka scheme. The Mori–Tanaka scheme [31,32] for estimating the effective moduli is applicable to regions of the graded microstructure that have a well-defined continuous matrix and a discontinuous particulate phase. It takes into account the interaction of the elastic fields among neighboring inclusions. It is assumed that the matrix phase, denoted by the subscript m, is reinforced by spherical particles of a particulate phase, denoted by the subscript c. In this notation, K_m and G_m are the bulk modulus and the shear modulus, respectively, and V_m is the volume fraction of the matrix phase. K_c, G_c, and V_c are the corresponding material properties and the volume fraction of the particulate phase. Note that $V_m + V_c = 1$, that the Lamé constant λ is related to the bulk and the shear moduli by $\lambda = K - 2G/3$, and that the stress–temperature modulus is related to the coefficient of thermal expansion by $\beta = (3\lambda + 2G)\alpha = 3K\alpha$. The following estimates for the effective local bulk modulus K and shear modulus G are useful for a random distribution of isotropic particles in an isotropic matrix:

$$\frac{K - K_m}{K_c - K_m} = \frac{V_c}{1 + (1 - V_c)(K_c - K_m)/(K_m + (4/3)K_m)}, \tag{2}$$

$$\frac{G - G_m}{G_c - G_m} = \frac{V_c}{1 + (1 - V_c)(G_c - G_m)/(G_m + f_m)} \tag{3}$$

where $f_m = G_m(9K_m + 8G_m)/6(K_m + 2G_m)$. The effective values of Young's modulus, E, and Poisson's ratio, v, are found from:

$$E = \frac{9KG}{3K+G}, \quad v = \frac{3K-2G}{2(3K+G)}. \tag{4}$$

Note that, in this paper, we choose a metal/ceramic open cylindrical shell with the metal (Al) taken as the matrix phase and the ceramic (SiC) taken as the particulate phase.

2.2 Problem description

The mechanical constitutive relations, which relate the stresses to the strains, are as follows:

$$\begin{bmatrix} \sigma_x \\ \sigma_\theta \\ \sigma_z \\ \tau_{z\theta} \\ \tau_{xz} \\ \tau_{x\theta} \end{bmatrix} = \begin{bmatrix} \bar{C}_{11} & \bar{C}_{12} & \bar{C}_{13} & 0 & 0 & 0 \\ \bar{C}_{12} & \bar{C}_{22} & \bar{C}_{23} & 0 & 0 & 0 \\ \bar{C}_{13} & \bar{C}_{23} & \bar{C}_{33} & 0 & 0 & 0 \\ 0 & 0 & 0 & \bar{C}_{44} & 0 & 0 \\ 0 & 0 & 0 & 0 & \bar{C}_{55} & 0 \\ 0 & 0 & 0 & 0 & 0 & \bar{C}_{66} \end{bmatrix} \begin{bmatrix} \varepsilon_x \\ \varepsilon_\theta \\ \varepsilon_z \\ \gamma_{z\theta} \\ \gamma_{xz} \\ \gamma_{x\theta} \end{bmatrix}. \tag{5}$$

In the absence of body forces, the governing equations are as follows:

$$\begin{aligned} &\frac{\partial \sigma_x}{\partial x} + \frac{1}{z}\frac{\partial \tau_{x\theta}}{\partial \theta} + \frac{\partial \tau_{zx}}{\partial z} + \frac{\tau_{zx}}{z} = \rho \frac{\partial^2 u_x}{\partial t^2}, \\ &\frac{\partial \tau_{\theta x}}{\partial x} + \frac{\partial \sigma_\theta}{z\partial \theta} + \frac{\partial \tau_{z\theta}}{\partial z} + \frac{2\tau_{z\theta}}{z} = \rho \frac{\partial^2 u_\theta}{\partial t^2}, \\ &\frac{\partial \tau_{xz}}{\partial x} + \frac{1}{z}\frac{\partial \tau_{\theta z}}{\partial \theta} + \frac{\partial \sigma_z}{\partial z} + \frac{\sigma_z - \sigma_\theta}{z} = \rho \frac{\partial^2 u_z}{\partial t^2}. \end{aligned} \tag{6}$$

The strain–displacement relations are expressed as:

$$\begin{aligned} &\varepsilon_\theta = \frac{u_z}{z} + \frac{\partial u_\theta}{z\partial \theta}, \quad \varepsilon_z = \frac{\partial u_z}{\partial z}, \quad \varepsilon_x = \frac{\partial u_x}{\partial x}, \quad \gamma_{z\theta} = \frac{-u_\theta}{z} + \frac{\partial u_\theta}{\partial z} + \frac{\partial u_z}{z\partial \theta}, \\ &\gamma_{xz} = \frac{\partial u_x}{\partial z} + \frac{\partial u_z}{\partial x}, \gamma_{x\theta} = \frac{\partial u_\theta}{\partial x} + \frac{\partial u_x}{z\partial \theta} \end{aligned} \tag{7}$$

where u_z, u_θ, and u_x are radial, circumferential, and axial displacement components, respectively.

Upon substituting Eq. (7) into (5) and then into (6), the following equations of motion in matrix form are obtained in terms of displacement components:

$$\begin{aligned} &\bar{C}_{55}\frac{\partial^2 u_x}{\partial z \partial x} + \bar{C}_{55}\frac{\partial^2 u_z}{\partial x^2} - \bar{C}_{44}\frac{1}{z^2}\frac{\partial u_\theta}{\partial \theta} + \bar{C}_{44}\frac{1}{z}\frac{\partial^2 u_\theta}{\partial z \partial \theta} + \bar{C}_{44}\frac{1}{z^2}\frac{\partial^2 u_z}{\partial \theta^2} + \frac{\partial \bar{C}_{13}}{\partial z}\frac{\partial u_x}{\partial x} + \bar{C}_{13}\frac{\partial^2 u_x}{\partial z \partial x} + \frac{\partial \bar{C}_{23}}{\partial z}\frac{1}{z}u_z \\ &+\frac{\partial \bar{C}_{23}}{\partial z}\frac{1}{z}\frac{\partial u_\theta}{\partial \theta} + \bar{C}_{23}\frac{1}{z}\frac{\partial^2 u_\theta}{\partial z \partial \theta} + \frac{\partial \bar{C}_{33}}{\partial z}\frac{\partial u_z}{\partial z} + \bar{C}_{33}\frac{\partial^2 u_z}{\partial z^2} + \bar{C}_{13}\frac{1}{z}\frac{\partial u_x}{\partial x} + \bar{C}_{33}\frac{1}{z}\frac{\partial u_z}{\partial z} - \bar{C}_{12}\frac{1}{z}\frac{\partial u_x}{\partial x} - \bar{C}_{22}\frac{1}{z^2}u_z \\ &-\bar{C}_{22}\frac{1}{z^2}\frac{\partial u_\theta}{\partial \theta} = \rho \frac{\partial^2 u_z}{\partial t^2}, \end{aligned} \tag{8}$$

$$\begin{aligned} &\bar{C}_{66}\frac{\partial^2 u_\theta}{\partial x^2} + \bar{C}_{66}\frac{1}{z}\frac{\partial^2 u_x}{\partial \theta \partial x} + \bar{C}_{12}\frac{1}{z}\frac{\partial^2 u_x}{\partial \theta \partial x} + \bar{C}_{22}\frac{1}{z^2}\frac{\partial u_z}{\partial \theta} + \bar{C}_{22}\frac{1}{z^2}\frac{\partial^2 u_\theta}{\partial \theta^2} + \bar{C}_{23}\frac{1}{z}\frac{\partial^2 u_z}{\partial z \partial \theta} - \frac{\partial \bar{C}_{44}}{\partial z}\frac{1}{z}u_\theta + \frac{\partial \bar{C}_{44}}{\partial z}\frac{\partial u_\theta}{\partial z} \\ &+\frac{\partial \bar{C}_{44}}{\partial z}\frac{1}{z}\frac{\partial u_z}{\partial \theta} + \bar{C}_{44}\frac{\partial^2 u_\theta}{\partial z^2} + \bar{C}_{44}\frac{1}{z}\frac{\partial^2 u_z}{\partial z \partial \theta} - \bar{C}_{44}\frac{1}{z^2}u_\theta + \bar{C}_{44}\frac{1}{z}\frac{\partial u_\theta}{\partial z} + \bar{C}_{44}\frac{1}{z^2}\frac{\partial u_z}{\partial \theta} = \rho \frac{\partial^2 u_\theta}{\partial t^2}, \end{aligned} \tag{9}$$

$$\begin{aligned} &\bar{C}_{11}\frac{\partial^2 u_x}{\partial x^2} + \bar{C}_{12}\frac{1}{z}\frac{\partial u_z}{\partial x} + \bar{C}_{12}\frac{1}{z}\frac{\partial^2 u_\theta}{\partial \theta \partial x} + \bar{C}_{13}\frac{\partial^2 u_z}{\partial z \partial x} + \bar{C}_{66}\frac{1}{z}\frac{\partial^2 u_\theta}{\partial \theta \partial x} + \bar{C}_{66}\frac{1}{z^2}\frac{\partial^2 u_x}{\partial \theta^2} + \frac{\partial \bar{C}_{55}}{\partial z}\frac{\partial u_x}{\partial z} \\ &+\frac{\partial \bar{C}_{55}}{\partial z}\frac{\partial u_z}{\partial x} + \bar{C}_{55}\frac{\partial^2 u_x}{\partial z^2} + \bar{C}_{55}\frac{\partial^2 u_z}{\partial z \partial x} + \bar{C}_{55}\frac{1}{z}\frac{\partial u_x}{\partial z} + \bar{C}_{55}\frac{1}{z}\frac{\partial u_z}{\partial x} = \rho \frac{\partial^2 u_x}{\partial t^2}. \end{aligned} \tag{10}$$

The outer and inner surfaces of the open cylindrical shell in the state of free vibration are traction free as:

$$\sigma_z = \tau_{zx} = \tau_{z\theta} = 0, \quad \text{at} \quad z = a \text{ and } b. \tag{11}$$

The surface boundary conditions in the state of static loading are:

$$\sigma_z = \tau_{zx} = \tau_{z\theta} = 0, \quad \text{at} \quad z = a. \tag{12}$$

$$\sigma_z = \tau_{zx} = \tau_{z\theta} = 0, \quad \text{at} \quad z = b. \tag{13}$$

In this investigation, the following boundary conditions for Simply (S) supported, Clamped (C) supported, Free (F) from support at the $x = 0, L_x$ edges are assumed:

$$\begin{aligned} S &: u_z = u_\theta = \sigma_x = 0, \\ C &: u_z = u_\theta = u_x = 0, \\ F &: \sigma_x = \sigma_{x\theta} = \sigma_{xz} = 0. \end{aligned} \tag{14}$$

For an open cylindrical shell with simply supported edge at one pair of opposite edges, the displacement components can be expanded in terms of trigonometric functions in the direction normal to these edges. In this work, it is assumed that the edges $\theta = 0$ and $\theta = \Psi$ are simply supported. Hence,

$$\begin{aligned} u_x(x,\theta,z,t) &= \sum_{m=1}^{\infty} U_x(x,z)\sin(\beta_m\theta)e^{i\omega t}, \\ u_\theta(x,\theta,z,t) &= \sum_{m=1}^{\infty} U_\theta(x,z)\cos(\beta_m\theta)e^{i\omega t}, \\ u_z(x,\theta,z,t) &= \sum_{m=1}^{\infty} U_z(x,z)\sin(\beta_m\theta)e^{i\omega t}, \\ \beta_m &= m\pi/\Psi, (m = 1, 2, \ldots,) \end{aligned} \tag{15}$$

where m and ω are circumferential wave number and natural angular frequency of the vibration.

Upon substituting Eq. (15) into the governing Eqs. (8)–(10), the coupled partial differential equations reduce to a set of ordinary differential relations as follows:

$$\begin{bmatrix} A_{1x} & A_{1\theta} & A_{1z} \\ A_{2x} & A_{2\theta} & A_{2z} \\ A_{3x} & A_{3\theta} & A_{3z} \end{bmatrix} \begin{Bmatrix} U_x \\ U_\theta \\ U_z \end{Bmatrix} = -\omega^2\rho \begin{Bmatrix} U_x \\ U_\theta \\ U_z \end{Bmatrix}, \tag{16}$$

where the coefficients A_{ij} are given in Appendix A.

3 Solution procedure

It is necessary to develop appropriate methods to investigate the mechanical responses of isotropic 2-D FGM structures. But, due to the complexity of the problem caused by the two-directional inhomogeneity, it is difficult to obtain the exact solution. In this paper, the generalized differential quadrature method (GDQM) approach is used to solve the governing equations of 2-D FGM open cylindrical shells. The basic idea of the GDQM is that the derivative of a function, with respect to a space variable at a given sampling point, is approximated as a weighted linear sum of the sampling points in the domain of that variable. According to GDQM method, the rth derivative of function $f(\xi, \eta)$ can be approximated as:

$$\left.\frac{\partial^r f(\xi,\eta)}{\partial\xi^r}\right|_{(\xi_i,\eta_i)} = \sum_{k=1}^{N_\xi} c_{ik}^{(r)} f(\xi_k,\eta_j) = \sum_{k=1}^{N_\xi} c_{ik}^{(r)} f_{kj}, i = 1, 2, \ldots, N_\xi \quad \text{and} \quad r = 1, 2, \ldots, N_\xi - 1. \tag{17}$$

From this equation, one can deduce that the important components of GDQM approximations are the weighting coefficients $c_{ij}^{(r)}$ and the choice of sampling points. Some simple recursive formulas are available for calculating

nth order derivative weighting coefficients $c_{ij}^{(r)}$ by means of Lagrange polynomial interpolation functions. The weighting coefficients for the first-order derivative, that is, $r = 1$, are [33,34]:

$$c_{ij}^{(1)} = \frac{L^{(1)}(\xi_i)}{(\xi_i - \xi_j)L^{(1)}(\xi_i)}, \quad i, j = 1, 2, \ldots, N_\xi, \quad i \neq j, \tag{18}$$

$$c_{ii}^{(r)} = -\sum_{j=1, i\neq j}^{N_\xi} c_{ij}^{(r)}. \tag{19}$$

In Eq. (18), the first derivative of the Lagrange interpolating polynomials at each point $\xi_i, i = 1, 2, \ldots, N_\xi$, is:

$$L^{(1)}(\xi_i) = \prod_{j=1, i\neq j}^{N} (\xi_i - \xi_j). \tag{20}$$

For higher-order derivatives ($r = 2, 3, \ldots, N_\xi - 1$), one can use the following relations iteratively:

$$c_{ij}^{(r)} = r\left(c_{ii}^{(r-1)} c_{ij}^{(1)} - \frac{c_{ij}^{(r-1)}}{(\xi_i - \xi_j)}\right) \quad i, j = 1, 2, \ldots, N_\xi, \quad i \neq j, \quad r = 2, 3, \ldots, N_\xi - 1, \tag{21}$$

$$c_{ii}^{(r)} = -\sum_{j=1, i\neq j}^{N_\xi} c_{ij}^{(r)}, \quad i = 1, 2, \ldots, N_\xi, \quad r = 1, 2, \ldots, N_\xi - 1. \tag{22}$$

A simple and natural choices of the grid distribution is the uniform grid spacing rule. However, it was found that non-uniform grid spacing yields result with better accuracy [35]. It has been proven that for the Lagrange interpolating polynomials the Chebyshev–Gauss–Lobatto sampling points rule guarantees convergence and efficiency to the GDQM technique [34,35]. Hence, in this work, the Chebyshev–Gauss–Lobatto quadrature points are used, that is [33],

$$\xi_i = \frac{1}{2}\left(1 - \cos\left(\frac{i-1}{N_\xi - 1}\pi\right)\right), \eta_j = \frac{1}{2}\left(1 - \cos\left(\frac{j-1}{N_\eta - 1}\pi\right)\right), \quad i = 1, 2, \ldots, N_\xi \text{ and } j = 1, 2, \ldots, N_\eta. \tag{23}$$

3.1 Free vibration problem

For free vibration analysis, the GDQM can be applied to discretize the equations of motion (16) and the boundary conditions (11) and (14). As a result, at each domain grid point (x_i, z_j) with $i = 1, 2, \ldots, N$ and $j = 1, 2, \ldots, M$, the discretized equations take the following forms:

$$\begin{aligned}
&\sum_{k=1}^{M}\left(\left(\frac{\partial \bar{C}_{11}}{\partial x}\right)_{ij} d_{jk} + \left(\bar{C}_{11}\right)_{ij} d_{jk}^{(2)}\right)U_{xik} + \left(\frac{\partial \bar{C}_{12}}{\partial x}\right)_{ij}\frac{1}{z}U_{zij} + \left(\left(\bar{C}_{12}\right)_{ij}\frac{1}{z} + \left(\bar{C}_{55}\right)_{ij}\frac{1}{z}\right.\\
&\quad\left. + \left(\frac{\partial \bar{C}_{55}}{\partial z}\right)_{ij}\right)\sum_{k=1}^{M} d_{jk}U_{zik} + \left(\left(\frac{\partial \bar{C}_{55}}{\partial z}\right)_{ij} + \left(\bar{C}_{55}\right)_{ij}\frac{1}{z}\right)\sum_{k=1}^{N} c_{ik}U_{xkj}\\
&\quad + \sum_{k=1}^{N}\left(\left(\frac{\partial \bar{C}_{13}}{\partial x}\right)_{ij} c_{ik} + \left(\bar{C}_{55}\right)_{ij} c_{ik}^{(2)}\right)U_{zkj}\\
&\quad - \left(\frac{\partial \bar{C}_{12}}{\partial x}\right)_{ij}\frac{1}{z}\beta_m U_{\theta ij} - \left(\bar{C}_{66}\right)_{ij}\frac{1}{z^2}\beta_m^2 U_{xij} - \frac{1}{z}\beta_m\left(\left(\bar{C}_{12}\right)_{ij} + \left(\bar{C}_{66}\right)_{ij}\right)\sum_{k=1}^{M} d_{jk}U_{\theta ik}\\
&\quad + \left(\left(\bar{C}_{55}\right)_{ij} + \left(\bar{C}_{13}\right)_{ij}\right)\sum_{k_1=1}^{N}\sum_{k_2=1}^{M} c_{ik_1}d_{jk_2}U_{zk_1k_2} = -\rho_{ij}\omega^2 U_{xij},
\end{aligned} \tag{24}$$

$$\sum_{k=1}^{M}\left(\left(\frac{\partial \bar{C}_{66}}{\partial x}\right)_{ij} d_{jk} + \left(\bar{C}_{66}\right)_{ij} d_{jk}^{(2)}\right) U_{\theta ik} + \sum_{k=1}^{N}\left(\left(\left(\frac{\partial \bar{C}_{44}}{\partial z}\right)_{ij} + \left(\bar{C}_{44}\right)_{ij}\frac{1}{z}\right) c_{ik} + \left(\bar{C}_{44}\right)_{ij} c_{ik}^{(2)}\right) U_{\theta kj}$$
$$+\left(\left(\bar{C}_{22}\right)_{ij}\frac{1}{z} + \left(\frac{\partial \bar{C}_{44}}{\partial z}\right)_{ij} + \left(\bar{C}_{44}\right)_{ij}\frac{1}{z}\right)\frac{1}{z}\beta_m U_{zij} + \left(\frac{\partial \bar{C}_{66}}{\partial x}\right)_{ij}\frac{1}{z}\beta_m U_{xij}$$
$$+\frac{1}{z}\beta_m \sum_{k=1}^{M}\left(\left(\bar{C}_{66}\right)_{ij} d_{jk}^{(2)} + \left(\bar{C}_{12}\right)_{ij} d_{jk}\right) U_{xik}$$
$$-\left(\left(\bar{C}_{22}\right)_{ij}\frac{1}{z^2}\beta_m^2 U_\theta + \left(\bar{C}_{44}\right)_{ij}\frac{1}{z^2}\right) U_{\theta ij} + \frac{1}{z}\beta_m\left(\left(\bar{C}_{23}\right)_{ij} + \left(\bar{C}_{44}\right)_{ij}\right)\sum_{k=1}^{N} c_{ik} U_{zkj} = -\rho_{ij}\omega^2 U_{\theta ij}, \tag{25}$$

$$\left(\left(\bar{C}_{13}\right)_{ij}\frac{1}{z} - \left(\bar{C}_{12}\right)_{ij}\frac{1}{z} + \left(\frac{\partial \bar{C}_{13}}{\partial z}\right)_{ij}\right)\sum_{k=1}^{M} d_{jk} U_{xik}$$
$$+\sum_{k=1}^{N}\left(\left(\left(\frac{\partial \bar{C}_{33}}{\partial z}\right)_{ij} + \left(\bar{C}_{33}\right)_{ij}\frac{1}{z}\right) c_{ik} + \left(\bar{C}_{33}\right)_{ij} c_{ik}^{(2)}\right) U_{zkj}$$
$$+\sum_{k=1}^{M}\left(\left(\frac{\partial \bar{C}_{55}}{\partial x}\right)_{ij} d_{jk} + \left(\bar{C}_{55}\right)_{ij} d_{jk}^{(2)}\right) U_{zik} + \beta_m\left(\left(\bar{C}_{44}\right)_{ij}\frac{1}{z^2} - \left(\frac{\partial \bar{C}_{23}}{\partial z}\right)_{ij}\frac{1}{z} + \left(\bar{C}_{22}\right)_{ij}\frac{1}{z^2}\right) U_{\theta ij}$$
$$+\left(\left(\frac{\partial \bar{C}_{23}}{\partial z}\right)_{ij}\frac{1}{z} - \left(\bar{C}_{44}\right)_{ij}\frac{1}{z^2}\beta_m^2 - \left(\bar{C}_{22}\right)_{ij}\frac{1}{z^2}\right) U_{zij} + \left(\left(\bar{C}_{13}\right)_{ij} + \left(\bar{C}_{55}\right)_{ij}\right)\sum_{k_1=1}^{N}\sum_{k_2=1}^{M} c_{ik_1} d_{jk_2} U_{xk_1k_2}$$
$$+\left(\frac{\partial \bar{C}_{55}}{\partial x}\right)_{ij}\sum_{k=1}^{N} c_{ik} U_{xkj} - \frac{1}{z}\beta_m\left(\left(\bar{C}_{44}\right)_{ij} + \left(\bar{C}_{23}\right)_{ij}\right)\sum_{k=1}^{N} c_{ik} U_{\theta kj} = -\rho_{ij}\omega^2 U_{zij} \tag{26}$$

where c_{ij}, d_{ij} and $c_{ij}^{(2)}$, $d_{ij}^{(2)}$ are the first- and second-order GDQM weighting coefficients in the z- and x-directions, respectively. In a similar manner, the boundary conditions can be discretized. For this purpose, using Eq. (11) and the GDQM discretization rule for special derivatives, the boundary conditions at $z = a$ and $z = b$ become:

$$\bar{C}_{13}\sum_{k=1}^{M} d_{jk} U_{xik} + \bar{C}_{23}\frac{1}{z} U_{rij} - \bar{C}_{23}\frac{1}{z}\beta_m U_{\theta ij} + \bar{C}_{33}\sum_{k=1}^{N} c_{ik} U_{zkj} = 0$$
$$-\bar{C}_{44}\frac{1}{z} U_{\theta ij} + \bar{C}_{44}\sum_{k=1}^{N} c_{ik} U_{\theta kj} + \bar{C}_{44}\frac{1}{z}\beta_m U_{zij} = 0, \tag{27}$$
$$\bar{C}_{55}\sum_{k=1}^{N} c_{ik} U_{xkj} + \bar{C}_{55}\sum_{k=1}^{M} d_{jk} U_{zik} = 0$$

where $i = 1$ at $z = a$ and $i = N$ at $z = b$, and $j = 1, 2, \ldots, M$. The boundary conditions at $x = 0$ and L stated in (14) become:

Simply supported (S):

$$U_{zij} = 0, \quad U_{\theta ij} = 0, \tag{28}$$
$$\bar{C}_{11}\sum_{k=1}^{M} d_{jk} U_{xik} + \bar{C}_{12}\frac{1}{z} U_{zij} - \bar{C}_{12}\frac{1}{z}\beta_m U_{\theta ij} + \bar{C}_{13}\sum_{k=1}^{N} c_{ik} U_{zkj} = 0, \quad \text{for} j = 1, M \quad \text{and} \quad i = 1, 2, \ldots, N.$$

Clamped (C):

$$U_{zij} = 0, \quad U_{\theta ij} = 0, \quad U_{xij} = 0, \quad \text{for} \quad j = 1, M \quad \text{and} \quad i = 1, 2, \ldots, N. \tag{29}$$

Free (F):

$$\begin{aligned}
&\bar{C}_{11}\sum_{k=1}^{M} d_{jk}U_{xik} + \bar{C}_{12}\frac{1}{z}U_{zij} - \bar{C}_{12}\frac{1}{z}\beta_m U_{\theta ij} + \bar{C}_{13}\sum_{k=1}^{N} c_{ik}U_{zkj} = 0,\\
&\bar{C}_{66}\sum_{k=1}^{M} d_{jk}U_{\theta ik} + \bar{C}_{66}\frac{1}{z}\beta_m U_{xij} = 0,\\
&\bar{C}_{55}\sum_{k=1}^{N} c_{ik}U_{xkj} + \bar{C}_{55}\sum_{k=1}^{M} d_{jk}U_{zik} = 0, \qquad \text{for } j = 1, M \quad \text{and} \quad i = 1, 2, \ldots, N.
\end{aligned} \tag{30}$$

To obtain the eigenvalue system of equations, the degrees of freedom are separated into the domain and the boundary degrees of freedom as

$$d = \begin{Bmatrix} U_x \\ U_\theta \\ U_z \end{Bmatrix}_{\text{domain}}, \quad b = \begin{Bmatrix} U_x \\ U_\theta \\ U_z \end{Bmatrix}_{\text{boundary}}. \tag{31}$$

Using Eq. (31), the discretized form of the equations of motion in matrix form can be rearranged as

$$\mathbf{S_{db}b} + \mathbf{S_{dd}d} = -\omega^2\mathbf{Md} \tag{32}$$

where $\mathbf{S_{db}}$ and $\mathbf{S_{dd}}$ are stiffness matrices and $\mathbf{M}$ is the mass matrix. In a similar manner, the discretized form of the boundary conditions becomes:

$$\mathbf{S_{bb}b} + \mathbf{S_{bd}d} = 0 \tag{33}$$

where $\mathbf{S_{bb}}$ and $\mathbf{S_{bd}}$ are the stiffness matrices. In the above equations, the elements of stiffness matrices are obtained based on the definition of vectors of domain and boundary degrees of freedom from the generalized differential quadrature discretized form of the equations of motion and the boundary conditions. Using Eq. (33) to eliminate the boundary degrees of freedom $\mathbf{b}$ from Eq. (32), one obtains

$$\mathbf{Sd} = -\omega^2\mathbf{Md} \tag{34}$$

where

$$\mathbf{S} = \mathbf{S_{dd}} - \mathbf{S_{db}}\mathbf{S_{bb}^{-1}}\mathbf{S_{bd}}.$$

The natural frequencies of the isotropic 2-D FGM open cylindrical shell considered can be determined by solving the standard eigenvalue problem (34).

3.2 Static problem

For the static analysis of a 2-D FGM open cylindrical shell, it is assumed that $\omega = 0$ in Eqs. (24)–(25). The discretized forms of the boundary conditions on the inner and outer surfaces of the open cylindrical shell, shown in Eqs. (12), (13), can be expressed as follows. On the inner surface ($z = a$):

$$\begin{aligned}
&\bar{C}_{13}\sum_{k=1}^{M} d_{jk}U_{xik} + \bar{C}_{23}\frac{1}{z}U_{rij} - \bar{C}_{23}\frac{1}{z}\beta_m U_{\theta ij} + \bar{C}_{33}\sum_{k=1}^{N} c_{ik}U_{zkj} = 0.\\
&-\bar{C}_{44}\frac{1}{z}U_{\theta ij} + \bar{C}_{44}\sum_{k=1}^{N} c_{ik}U_{\theta kj} + \bar{C}_{44}\frac{1}{z}\beta_m U_{zij} = 0.\\
&\bar{C}_{55}\sum_{k=1}^{N} c_{ik}U_{xkj} + \bar{C}_{55}\sum_{k=1}^{M} d_{jk}U_{zik} = 0.
\end{aligned} \tag{35}$$

On the outer surface ($z = b$):

$$\begin{aligned}
&\bar{C}_{13}\sum_{k=1}^{M} d_{jk}U_{xik} + \bar{C}_{23}\frac{1}{z}U_{rij} - \bar{C}_{23}\frac{1}{z}\beta_m U_{\theta ij} + \bar{C}_{33}\sum_{k=1}^{N} c_{ik}U_{zkj} = q,\\
&-\bar{C}_{44}\frac{1}{z}U_{\theta ij} + \bar{C}_{44}\sum_{k=1}^{N} c_{ik}U_{\theta kj} + \bar{C}_{44}\frac{1}{z}\beta_m U_{zij} = 0,\\
&\bar{C}_{55}\sum_{k=1}^{N} c_{ik}U_{xkj} + \bar{C}_{55}\sum_{k=1}^{M} d_{jk}U_{zik} = 0.
\end{aligned} \tag{36}$$

Applying the generalized differential quadrature procedure, the whole system of differential equations has been discretized, and the global assembling leads to the following set of linear algebraic equations:

$$\begin{bmatrix} \mathbf{S_{bb}} & \mathbf{S_{bd}} \\ \mathbf{S_{db}} & \mathbf{S_{dd}} \end{bmatrix} \begin{Bmatrix} \mathbf{b} \\ \mathbf{d} \end{Bmatrix} = \begin{Bmatrix} \mathbf{q} \\ 0 \end{Bmatrix} \tag{37}$$

where $\mathbf{q}$ is the mechanical load. Finally, the displacement components are obtained from the following relations:

$$\mathbf{Sd} = \mathbf{S_{db}}\mathbf{S_{bb}^{-1}}\mathbf{q} \tag{38}$$

where

$$\mathbf{S} = \mathbf{S_{db}}\mathbf{S_{bb}^{-1}}\mathbf{S_{bd}} - \mathbf{S_{dd}}. \tag{39}$$

The above system of equations can be solved to find the displacement fields of the metal/ceramic 2-D FGM open cylindrical shells.

4 Numerical results and discussion

To validate the vibration analyses, the numerical results for simply supported conventional FGM open cylindrical shells with different L_x/Z_m and L_x/h ratios shown in Table 2 are compared with those presented by Matsunaga [36] and Farid et al. [37].

In Table 3, the fundamental frequencies of the radially conventional FGM open cylindrical shell with four edges simply supported obtained by the present analysis are compared with those presented by Pradyumna and Bandyopadhyay [38], based on the higher-order shear deformation theory. The results of the present analysis are obtained using 9×9 grid points. Again, excellent agreement of the two methods is obvious.

Table 2 Comparison of the normalized natural frequency for various L_x/Z_m and L_x/h ratios

		P_z				
		0	0.5	1	4	10
$L_x/h = 2$	$L_x/Z_m = 0.5$					
Ref. [36]		0.9334	0.8213	0.7483	0.6011	0.5461
Ref. [37]		0.9187	0.8013	0.7263	0.5267	0.5245
Present results ($M = N = 9$)		0.9249	0.8018	0.7253	0.5790	0.5301
Ref. [36]	$L_x/Z_m = 1$	0.9163	0.8105	0.7411	0.5967	0.5392
Ref. [37]		0.8675	0.7578	0.6875	0.5475	0.4941
Present results ($M = N = 9$)		0.8857	0.7667	0.6935	0.5531	0.5065
$L_x/h = 5$	$L_x/Z_m = 0.5$					
Ref. [36]		0.2153	0.1855	0.1678	0.1413	0.1328
Ref. [37]		0.2113	0.1814	0.1639	0.1367	0.1271
Present results ($M = N = 9$)		0.2129	0.1817	0.1638	0.1374	0.1296
Ref. [36]	$L_x/Z_m = 1$	0.2239	0.1945	0.1769	0.1483	0.1385
Ref. [37]		0.2164	0.1879	0.1676	0.1394	0.1286
Present results ($M = N = 9$)		0.2154	0.1848	0.1671	0.1391	0.1300

Table 3 Comparison of the normalized natural frequency of a radially FGM open cylindrical shell with four edges simply supported for various γ_z and Z_m/L_x ratios

γ_z		Z_m/L_x				
		0.5	1	5	10	50
0	Ref. [38]	68.8645	51.5216	42.2543	41.908	41.7963
	$M = N = 5$	69.97756	52.10533	42.72019	42.37183	42.25946
	$M = N = 9$	69.97003	52.10028	42.716036	42.36770	42.25534
	$M = N = 11$	69.97003	52.10028	42.716036	42.36770	42.25534
0.2	Ref. [38]	64.4001	47.5968	40.1621	39.8472	39.7465
	$M = N = 5$	65.14701	47.93925	39.12822	38.80092	38.70198
	$M = N = 9$	65.45263	48.13411	39.08355	38.75680	38.65808
	$M = N = 11$	65.43035	48.13411	39.08355	38.75680	38.65808
0.5	Ref. [38]	59.4396	43.3019	37.287	36.9995	36.9088
	$M = N = 5$	60.11963	43.55386	36.12641	35.82024	34.73412
	$M = N = 9$	60.35742	43.76887	36.09438	35.78910	35.70322
	$M = N = 11$	60.35742	43.76887	36.09438	35.78910	35.70322
1	Ref. [38]	53.9296	38.7715	33.2268	32.9585	32.875
	$M = N = 5$	54.10335	38.51794	31.98603	30.70648	30.63364
	$M = N = 9$	54.71405	39.16213	32.04008	31.76079	31.68770
	$M = N = 11$	54.71405	39.16213	32.04008	31.76079	31.68770
2	Ref. [38]	47.8259	34.3338	27.4449	27.1789	27.0961
	$M = N = 5$	46.90162	34.77015	27.66574	27.42946	27.37254
	$M = N = 9$	48.52503	34.68517	27.56144	27.32382	27.26625
	$M = N = 11$	48.52503	34.68517	27.56144	27.32382	27.26625

$\left(\Omega = \omega Z_m \Phi \sqrt{\rho_m h/D},\ D = E_m h^3/\left(12(1-v_m^2)\right)\right)$

Table 4 Comparison of the maximum stresses for a 1-layer orthotropic cylindrical shell (N, $M = 13$, $L_x/Z_m = 4$)

S		$\bar{\sigma}_\theta$ $(\eta = \pm 0.5)$	$\bar{\sigma}_x$ $(\eta = \pm 0.5)$	$\bar{\sigma}_z$ $(\eta = 0)$	$\bar{\sigma}_{z\theta}$ $(\eta = 0)$
2	Present	−14.8825 5.163241	−0.78390 0.13317	−0.37409	−2.05563
	Ref. [39]	−14.883 5.163	−0.7839 0.1332	−0.37	−2.056
10	Present	−4.50902 4.05089	−0.06558 0.06632	−1.372343	−3.66901
	Ref. [39]	−4.509 4.051	−0.0656 0.0663	−1.37	−3.669
50	Present	−3.97856 3.90184	−0.00857 0.08447	−5.38282	−3.91932
	Ref. [39]	−3.979 3.902	−0.0086 0.0845	−5.38	−3.919
100	Present	−3.87638 3.84309	0.02878 0.11897	−10.12841	−3.85904
	Ref. [39]	−3.876 3.843	0.0288 0.119	−10.13	−3.859

To validate the static analysis, the present results are obtained for a 1-layer orthotropic cylindrical shell under internal static load and compared with similar results by Varadan [39]. The mechanical properties of the considered material are as follows:

$$\frac{E_L}{E_T} = 25, \quad \frac{G_{TT}}{E_T} = 0.2, \quad \frac{G_{LT}}{E_T} = 0.5, \quad v_{LT} = v_{TT} = 0.25. \tag{40}$$

The non-dimensional parameters are:

$$(\bar{\sigma}_x, \bar{\sigma}_\theta) = \frac{10(\sigma_x, \sigma_\theta)}{qS^2}, \quad \bar{\sigma}_z = \frac{\sigma_z}{q}, \quad \bar{\tau}_{z\theta} = \frac{10\tau_{z\theta}}{qS}. \tag{41}$$

As it is observed from Table 4, there is good agreement between the results.

Table 5 Various ceramic volume fraction profiles, different parameters, and volume fraction indices of 2-D power-law distributions

Volume fraction profile	Radial volume fraction index and parameters	Axial volume fraction index and parameters
Classical–Classical	$\alpha_z = 0$	$\alpha_x = 0$
Symmetric–Symmetric	$\alpha_z = 1, \beta_z = 2$	$\alpha_x = 1, \beta_x = 2$
Classical–Symmetric	$\alpha_z = 0$	$\alpha_x = 1, \beta_x = 2$
Classical radially	$\alpha_z = 0$	$\gamma_x = 0$
Symmetric radially	$\alpha_z = 1, \beta_z = 2$	$\gamma_x = 0$

Table 6 Convergence test of fundamental frequency parameters of a C-C 2-D FGM open cylindrical shell ($L_x/Z_m = 5$, $\Psi = \pi/2$)

Volume fraction profile	S	Number of grid points ($M \times N$)				
		9×9	13×13	15×15	17×17	21×21
Classical–Classical	10	0.020676	0.020602	0.020587	0.020570	0.020570
	20	0.009039	0.008969	0.008952	0.008947	0.008947
	50	0.003453	0.003417	0.003403	0.003397	0.003397
	100	0.001714	0.001696	0.001688	0.001683	0.001683
Classical–Symmetric	10	0.024938	0.024868	0.024854	0.024841	0.024841
	20	0.011005	0.010940	0.010924	0.010919	0.010919
	50	0.004219	0.004187	0.004174	0.004168	0.004168
	100	0.002095	0.002079	0.002071	0.002067	0.002067
Symmetric–Symmetric	10	0.028941	0.028885	0.028877	0.028870	0.028870
	20	0.012742	0.012682	0.012668	0.012666	0.012666
	50	0.004882	0.004851	0.004838	0.004834	0.004834
	100	0.002425	0.002409	0.002402	0.002398	0.002398

4.1 Free vibration problem

For all results presented here, the vibration frequency is expressed in terms of a non-dimensional frequency parameter $\Omega_{mn} = \omega_{mn} h\sqrt{\rho_{Al}/E_{Al}}$($\rho_{Al}$, E_{Al} are mechanical properties of aluminum). In this work, C–C, C–S, S–S, F–C, F–S, and F–F denote clamped–clamped, clamped–simply supported, simply supported–simply supported, free–clamped, free–simply supported and free–free conditions at the circumferential edges and simply supported axial pair of edges. It is should be noted that the isotropic 2-D FGM shells considered in the work are assumed to be composed of aluminum and silicon carbide. In the following, we have compared the several different ceramic volume fraction profiles of conventional 1-D and 2-D FGMs with appropriate choice of the radial and axial parameters of the 2-D six-parameter power-law distribution, as shown in Table 5. It should be noted that the notation *Classical–Symmetric* indicates that the 2-D FGM open cylindrical shell has classical and symmetric volume fraction profiles in the radial and axial directions, respectively. In order to obtain accurate frequency parameters of 2-D FGM open cylindrical shells, a set of calculations is first presented in Tables 6 and 7 to determine the requisite number of grid points in the radial M and axial N directions. The effect of the mid-radius-to-thickness ratio (S), length-to-mean radius ratio (L/Z_m), and various volume fraction profiles on the convergence rate of the frequency parameters of 2-D FGM open cylindrical shells is investigated in Tables 6 and 7, respectively. It is evident from these tables that the present GDQM converges very fast as the number of grid points $M \times N$ increases. It can also be concluded that using 17×17 grid points can produce accurate frequency parameters for 2-D FGM open cylindrical shells up to at least six significant digits.

The variations of the frequency parameters of FGM metal/ceramic open cylindrical shells with mid-radius-to-thickness ratio, S, and radial volume fraction index for the four boundary conditions are shown in Fig. 5, by considering $\alpha_z = \alpha_x = 0$ and $\gamma_x = 1$ for a *Classical–Classical* 2-D FGM. As it is observed, for the all boundary conditions the fundamental frequency parameter decreases rapidly with the increase in the S ratio and then remains almost unaltered for the thin shells. By considering the relations (1), when the radial volume fraction index γ_z is set equal to zero, the conventional 1-D FGM shell with the graded ceramic volume fraction graded in the radial direction is obtained as a special case of functionally graded material. It is interesting to note that for the all boundary conditions the frequency parameter decreases by increasing the radial volume fraction index γ_z, due to the fact that the silicon carbide fraction decreases, and as we know silicon carbide has a much higher Young's modulus than aluminum.

Table 7 Convergence behavior of fundamental frequency parameters of an F-C 2-D FGM open cylindrical shell against the number of grid points ($S = 10$, $\Psi = \pi/3$)

Volume fraction profile	L_x/Z_m	Number of grid points ($M \times N$)				
		9×9	13×13	15×15	17×17	21×21
Classical–Classical	1	0.047374	0.047374	0.047776	0.048244	0.048244
	2	0.035056	0.034572	0.034539	0.034916	0.034916
	5	0.030093	0.030091	0.030064	0.030084	0.030084
	10	0.026899	0.026935	0.026927	0.026923	0.026923
Classical–Symmetric	1	0.057001	0.056919	0.057027	0.057103	0.057103
	2	0.037921	0.037746	0.037714	0.037801	0.037801
	5	0.033563	0.033614	0.033616	0.033622	0.033622
	10	0.032509	0.032512	0.032513	0.032513	0.032513
Symmetric–Symmetric	1	0.068810	0.068317	0.068238	0.067990	0.067990
	2	0.045774	0.045499	0.045408	0.045350	0.045350
	5	0.039805	0.039833	0.039820	0.039811	0.039811
	10	0.037932	0.037929	0.037933	0.037934	0.037934

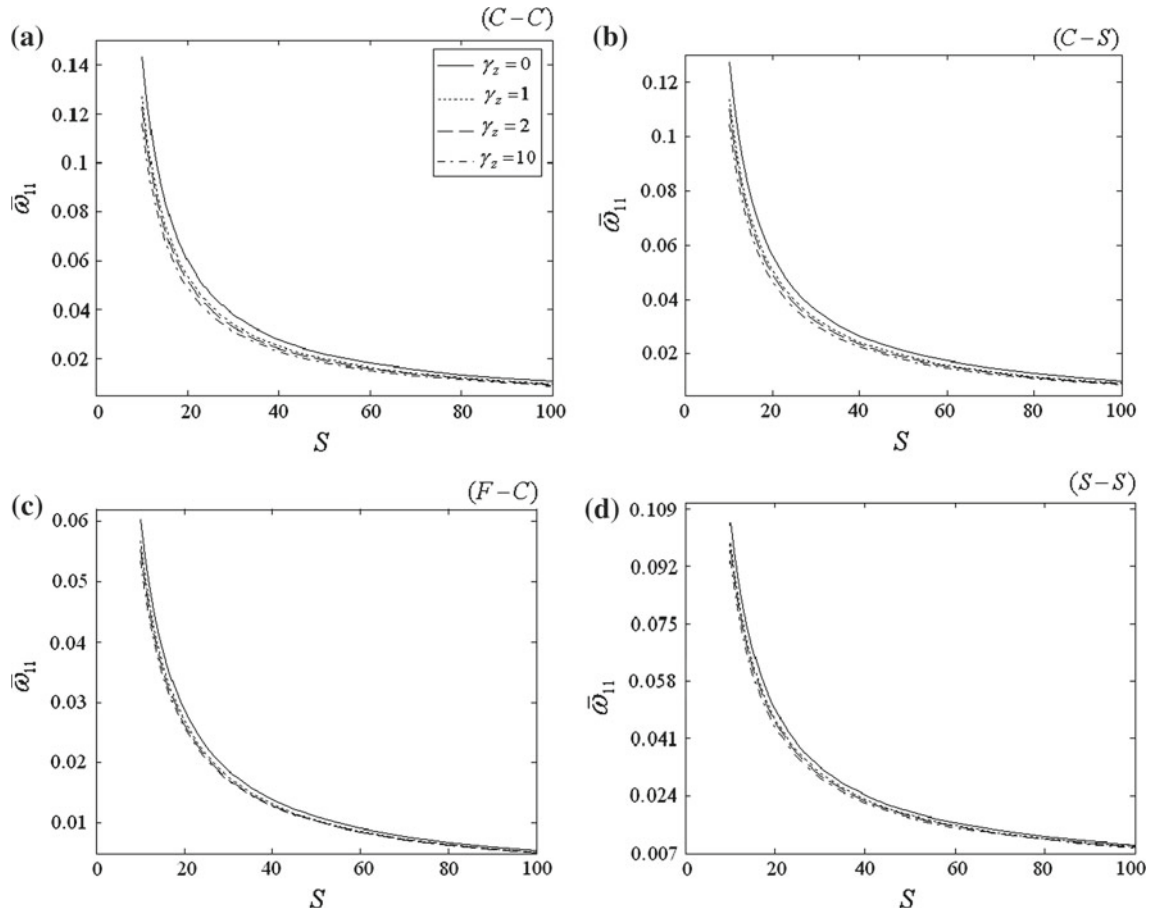

Fig. 5 Variations of the fundamental frequency parameters of FGM metal/ceramic open cylindrical shells with S ratio and radial volume fraction index for different boundary conditions ($\Psi = 2\pi/3$, $L_x/Z_m = 5$, $\alpha_z = \alpha_x = 0$, $\gamma_x = 1$)

The influence of various types of ceramic volume fraction profiles on the frequency parameters of C-C open cylindrical shells for different values of circumferential wave number m and length-to-mean radius ratio L_x/Z_m is shown in Figs. 6 and 7. According to Figs. 6 and 7, the lowest frequency parameter is obtained by using a *Classical–Classical* volume fractions profile. On the contrary, a 1-D FGM open cylindrical shell with *Symmetric* volume fraction profile has the maximum value of the frequency parameter. Therefore, a graded ceramic volume fraction in two directions has higher capabilities to reduce the frequency parameter than conventional 1-D FGM. In addition, the new results show that, for different values of the circumferential wave number m and

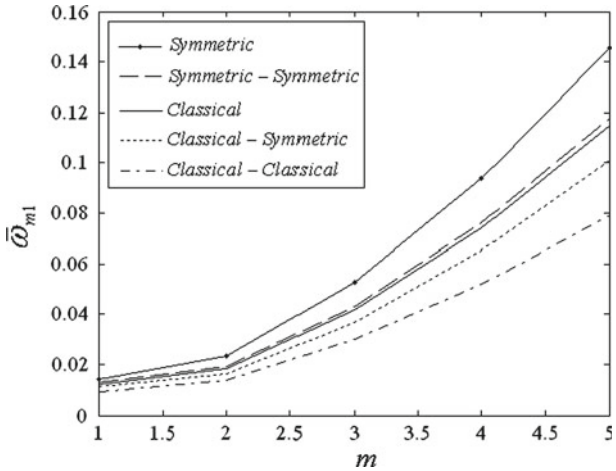

Fig. 6 Influence of various types of ceramic volume fraction profile on the frequency parameters of C–C open cylindrical shells for different values of the circumferential wave number m ($L_x/Z_m = 1$, $S = 20$, $\Psi = \pi/2$)

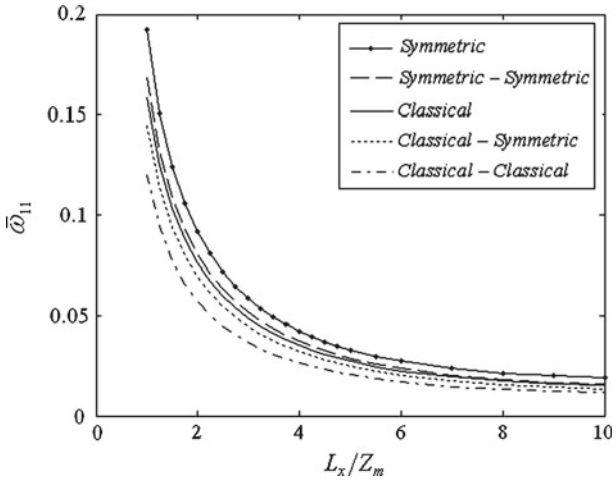

Fig. 7 Influence of various types of ceramic volume fraction profile on the fundamental frequency parameters of C–C open cylindrical shells ($S = 10$, $\Psi = \pi/2$)

ratio L_x/Z_m, the frequency parameter of the *Classical* FGM open cylindrical shell is close to that of a *Symmetric–Symmetric* 2-D FGM open cylindrical shell. Therefore, it can be concluded that using a 2-D power-law distribution leads to a more flexible design so that the maximum or minimum value of the natural frequency can be obtained in a required manner. It should be noted that the effect of the circumferential wave number m on the growth rate of the frequency parameter is more pronounced for the *Symmetric* and *Symmetric–Symmetric* volume fraction profiles.

The effects of different boundary conditions on the frequency parameters of 2-D FGM metal/ceramic open cylindrical shells with *Classical–Classical* profile for different values of circumferential wave numbers m are compared in Fig. 8. The frequency parameters vary from the maximum value for the C–C to the minimum value for the F–S one. Figure 8a–c shows, for different values of S ratio, that the effects of the boundary conditions diminish as the circumferential wave numbers m increase.

Here, we studied the influence of various types of the ceramic volume fraction profile on the fundamental natural frequency at various radial volume fraction indices γ_z (Fig. 9). As observed, the fundamental natural frequency decreases rapidly and then approaches a constant value for higher values of γ_z. It can be inferred from Fig. 9 that the radial volume fraction index γ_z exerts insignificant influence on the frequency parameter for the *Classical–Classical* volume fraction profile.

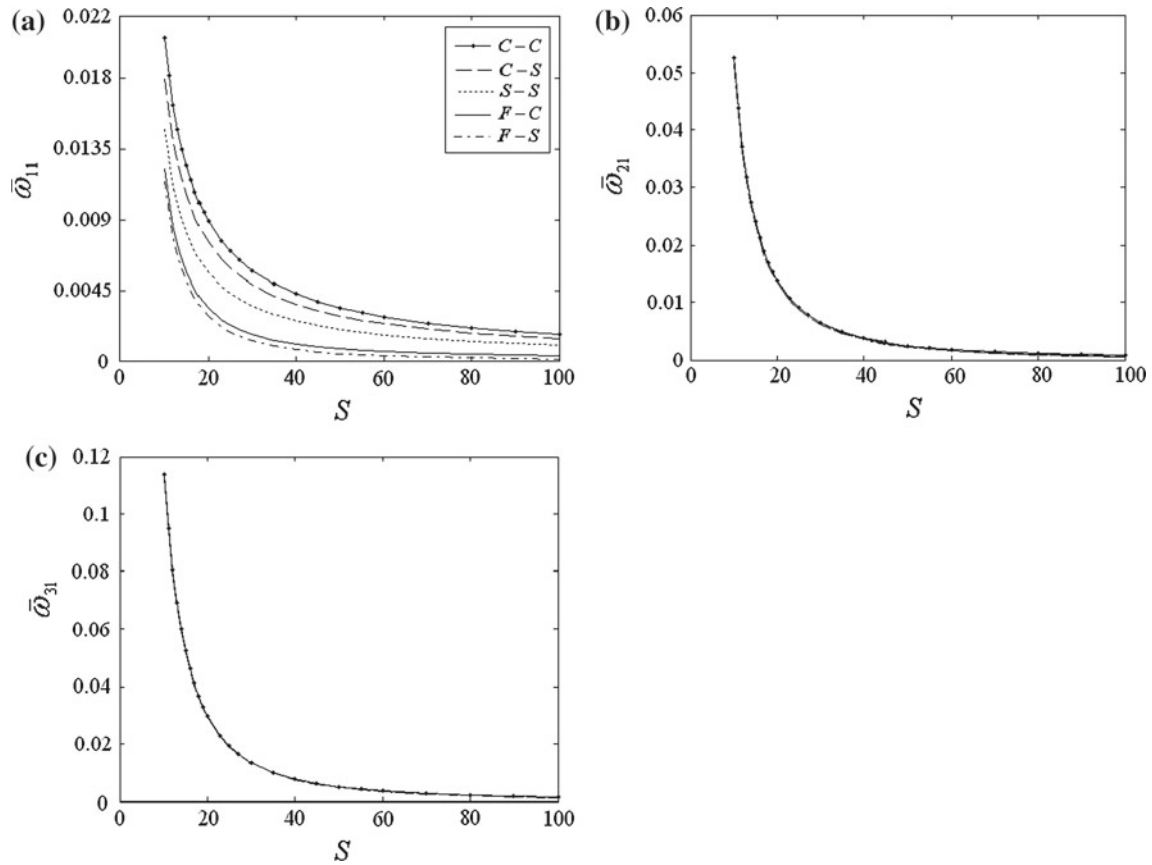

Fig. 8 Effect of various boundary conditions on the frequency parameters of a 2-D FGM metal/ceramic open cylindrical shell for different values of circumferential wave numbers m (**a** $m = 1$; **b** $m = 2$; **c** $m = 3$)($\Psi = \pi/2$, $L_x/Z_m = 5$)

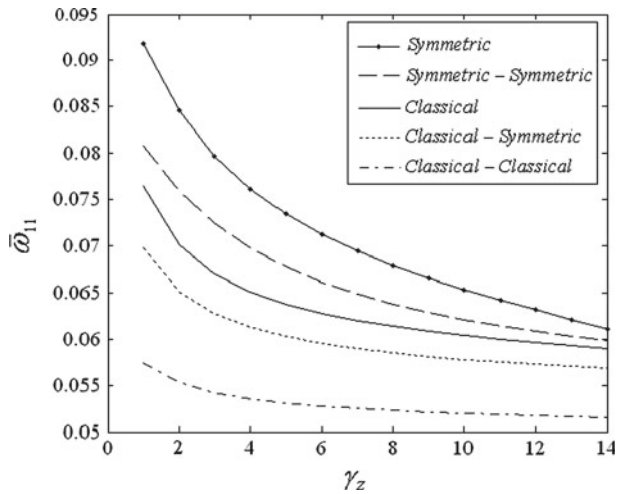

Fig. 9 Frequency variation against radial volume fraction index γ_z for a C–C FGM metal/ceramic open cylindrical shell ($\Psi = \pi/2$, $L_x/Z_m = 2$, $S = 10$)

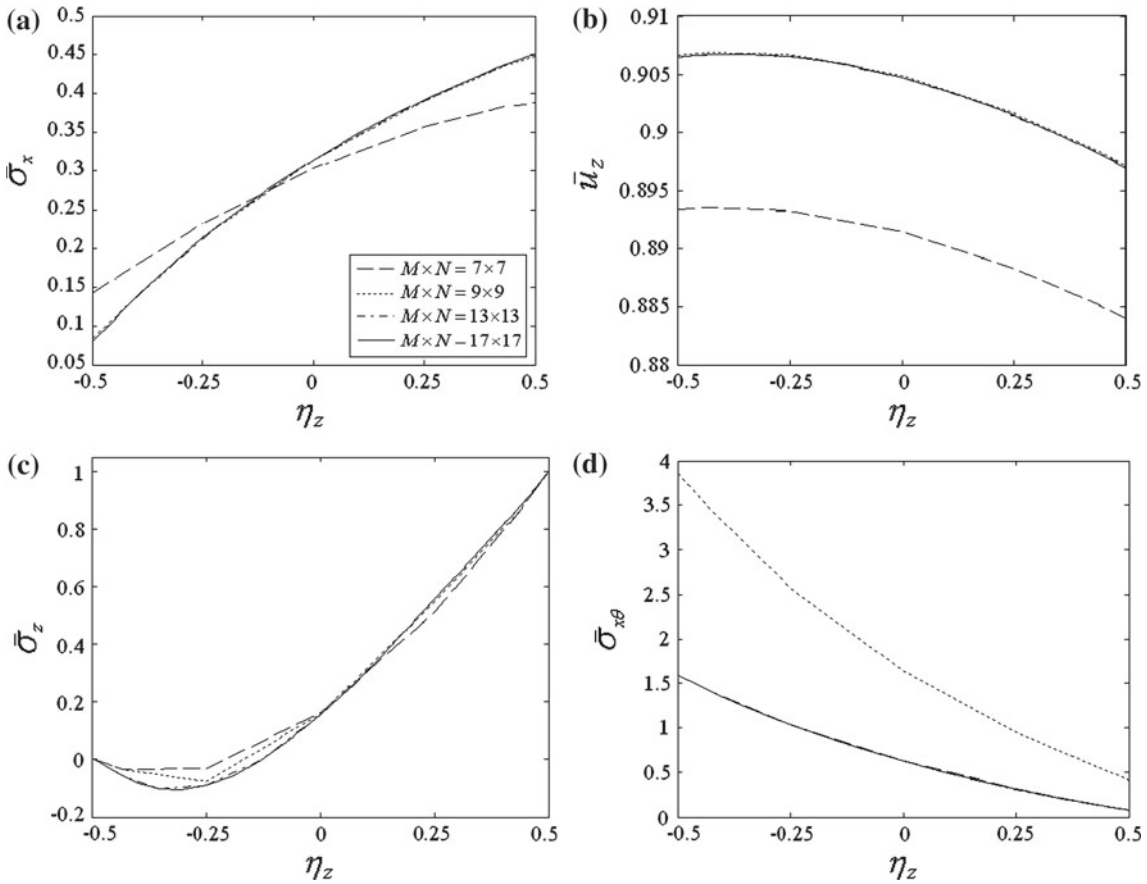

Fig. 10 Convergency of the non-dimensional radial displacement and radial, axial and transverse shear stresses through the thickness C–C open cylindrical shell for *Classical–Classical* 2-D FGM ($\Psi = 2\pi/3S = 5, \theta = \pi/3, z = L_x/2$)

4.2 Static problem

The displacement and stress components are non-dimensionalized as follows:

$$(\bar{\sigma}_z, \bar{\sigma}_{zx}, \bar{\sigma}_{z\theta}) = \frac{(\sigma_z, \sigma_{zx}, \sigma_{z\theta})}{q}, \quad (\bar{\sigma}_x, \bar{\sigma}_\theta) = \frac{(\sigma_x, \sigma_\theta)}{qS^2}, \quad \bar{U}_r = \frac{E_{Al}U_r}{qS^2}. \tag{42}$$

E_{Al} is a mechanical property of aluminum. The open cylindrical shell has geometrical parameters $L_x = 2\,\text{m}$, $Z_m = 0.5\,\text{m}$. A convergence study of the non-dimensional radial displacement and radial, axial, and transverse shear stresses through the thickness is shown in Fig. 10a–d, for *Classical–Classical* 2-D FGM. As observed, a fast rate of convergence of the method is evident, and it can also be seen that for the considered system the formulation is stable while increasing the number of points.

The influence of edge boundary conditions on the static behavior of a 2-D FGM open cylindrical shell are presented in Fig. 11a–d. As Fig. 11a shows, the two built-in opposite edges can cause the magnitude of radial stress to be minimum in comparison with the other boundary conditions. The magnitude of non-dimensional radial, circumferential, and transverse shear stresses for the 2-D FGM open cylindrical shell with F-C edges condition are larger than on the other boundary conditions. It is interesting to note that the effect of clamped condition in the opposite edges on the distribution of circumferential stress is less than on the other stresses (Fig. 11d).

The influence of radial volume fraction index γ_z on the non-dimensional radial, axial, and transverse shear stresses through the thickness is presented in Fig. 12a–c. The non-dimensionalized axial stress is linear for $\gamma_z = 0$. In Fig. 12b, it is seen that the non-dimensionalized axial stress on the inner and outer surfaces increases with increasing the radial volume fraction index. In this Fig. 12a and c, the peak of the radial and transverse shear stresses increases by decreasing ceramic matrix phase (with increasing the radial volume fraction index).

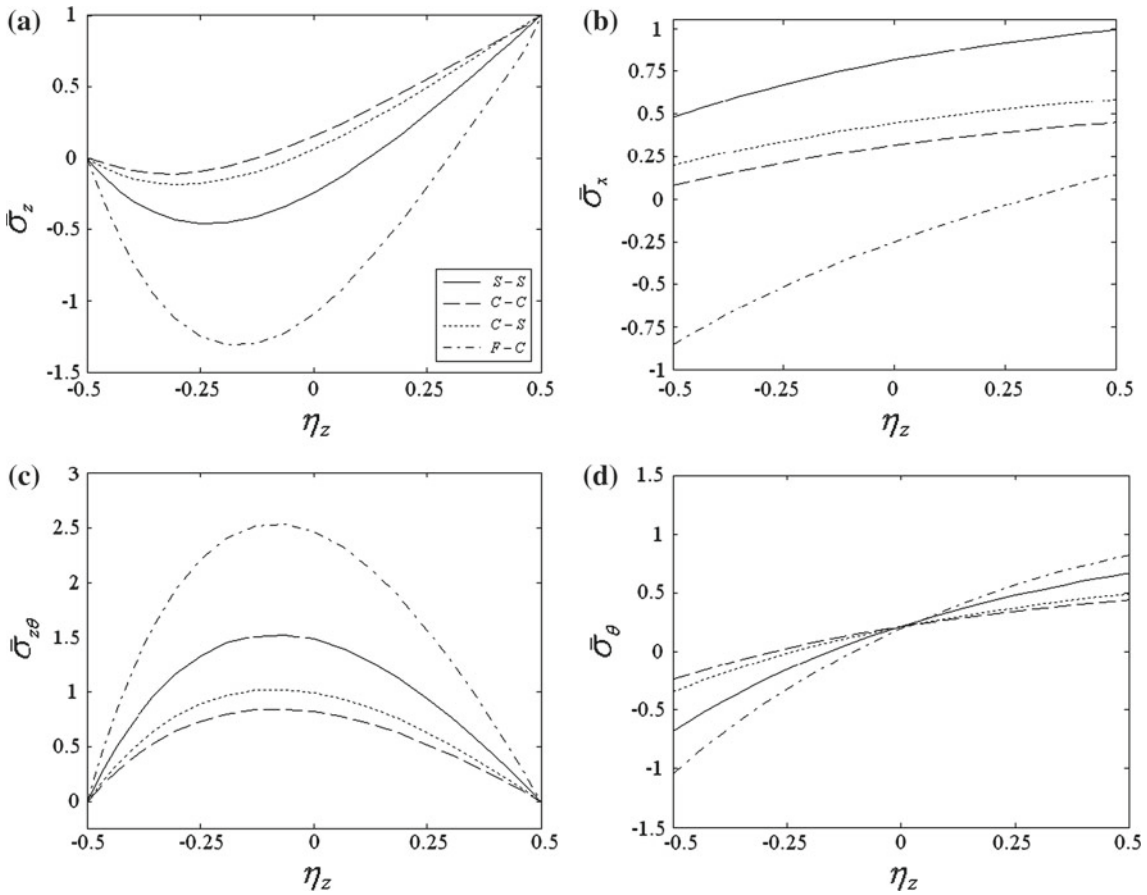

Fig. 11 Influence of edge boundary conditions on the mechanical entities of a 2-D FGM open cylindrical shell ($\Psi = 2\pi/3$, $S = 5, \theta = \pi/3$)

It can be seen, with the exception of $\gamma_z = 0$, that the distribution is not symmetric with respect to the mid-surface of the open cylindrical shell.

In the following discussion, the effect of different types of ceramic volume fraction profiles on the mechanical entities of an F-S 2-D FGM open cylindrical shell is compared in Fig. 13. According to Fig. 13a–c, the lowest magnitude of mechanical entities is obtained by using the *Classical–Classical* volume fractions profile. On the contrary, a 1-D FGM open cylindrical shell with *Classical* volume fraction profile has the maximum magnitude of mechanical entities. Therefore, a graded ceramic volume fraction in two directions has higher capabilities to reduce the mechanical stresses than conventional 1-D FGM. Moreover, in Fig. 13, it is interesting to note that the distribution of the mechanical entities in an FGM open cylindrical shell with *Symmetric* and *Symmetric–Symmetric* profiles is symmetric with respect to the mid-surface of the open cylindrical shell. It can be inferred from these figures that the 2-D power-law distribution for the ceramic volume fraction of 2-D FGM gives designers a powerful tool for flexible designing of structures under multifunctional requirements.

5 Conclusion remarks

In this research work, a theoretical formulation for the free vibration and static response of a 2-D functionally graded (2-D FGM) metal/ceramic open cylindrical shell under various boundary conditions was developed using the 2-D generalized differential quadrature method. This paper presented a novel 2-D power-law distribution for the ceramic volume fraction of 2-D FGM that gives designers a powerful tool for flexible designing of structures under multifunctional requirements. Various material profiles in two radial and axial directions were illustrated using the 2-D power-law distribution. The effective material properties at a point were determined in terms of the local volume fractions and the material properties by the Mori–Tanaka scheme. The study was

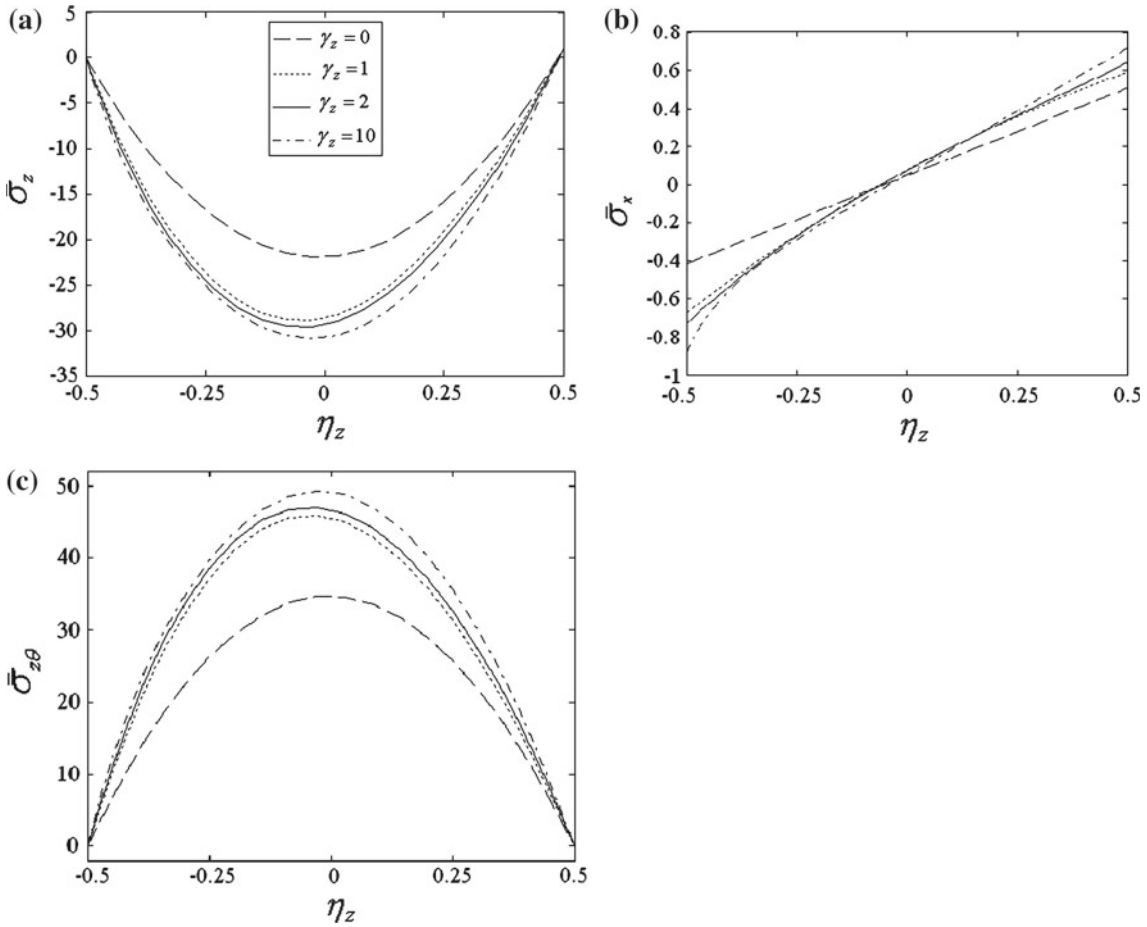

Fig. 12 Through-the-thickness variation of the mechanical entities for different values of the radial volume fraction index ($\Psi = \pi/2, S = 10, \theta = \pi/4, z = L_x/2$)

carried out based on the 3-D, linear and small strain elasticity theory. Open cylindrical shells with two opposite edges simply supported and arbitrary boundary conditions at the other edges were considered. The effects of different boundary conditions, various geometrical parameters, and different ceramic volume fraction profiles in radial and axial directions on the vibration and static behavior of 2-D FGM metal/ceramic open cylindrical shells were investigated. From this study, some conclusions can be made:

- The results show that the fundamental natural frequency decreases rapidly and then approaches a constant value for higher values of the radial volume fraction index. It is also seen that the radial volume fraction index exerts an insignificant influence on the frequency parameter for the *Classical–Classical* volume fraction profile.
- It is found that for the all boundary conditions the frequency parameter decreases by increasing radial volume fraction index, due to the fact that the silicon carbide fraction decreases, and as we know silicon carbide has a much higher Young's modulus than aluminum.
- Results indicate that using a 2-D power-law distribution leads to a more flexible design so that maximum or minimum mechanical stresses and a symmetric or asymmetric distribution can be obtained in a required manner.
- The interesting results show that the lowest magnitude of mechanical entities and frequency parameter is obtained by using a *Classical–Classical* volume fractions profile. It can be concluded that a graded ceramic volume fraction in two directions has higher capabilities to reduce the mechanical stresses and natural frequency than a conventional 1-D FGM.
- It is shown that the effect of clamped condition in the opposite edges on the distribution of circumferential stress is smaller than on the other stresses. Moreover, it is observed that the magnitude of non-dimensional

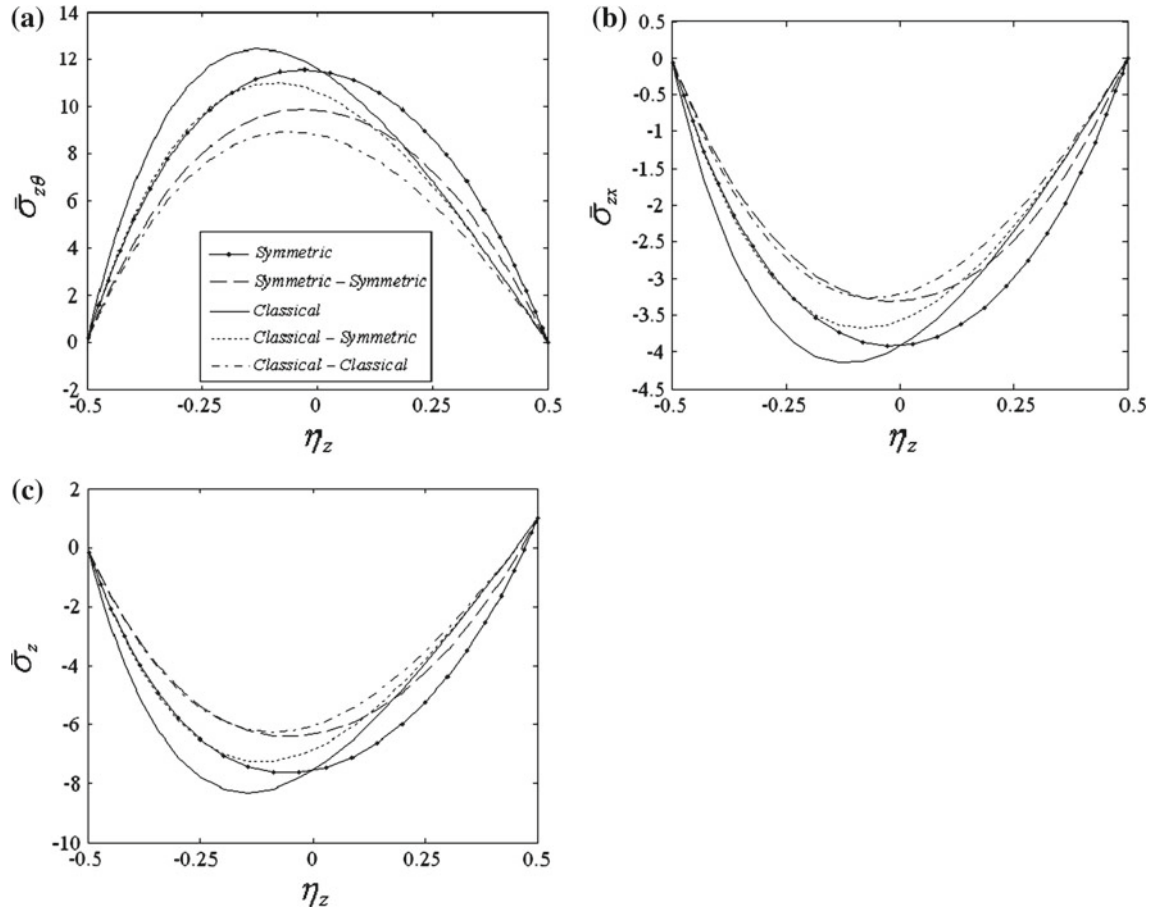

Fig. 13 The influence of the various ceramic volume fraction profiles on the mechanical entities of an F–S 2-D FGM open cylindrical shell ($\Psi = 2\pi/3$, $S = 10$, $\theta = \pi/3$, $z = L_x/2$)

radial, circumferential, and transverse shear stresses for the 2-D FGM open cylindrical shell with F–C edges condition is larger than for the other boundary conditions.

- The results show that the distribution of the mechanical entities in an FGM open cylindrical shell with *Symmetric* and *Symmetric–Symmetric* profiles is symmetric with respect to the mid-surface of the open cylindrical shell.
- Based on the achieved results, using a 2-D power-law distribution leads to a more flexible design so that maximum or minimum mechanical stresses and a symmetric or asymmetric distribution can be obtained in a required manner.

Appendix A: Expressions for the coefficients A_{ij} in Eq. (16):

$$A_{1z} = \left[\frac{\partial \bar{C}_{23}}{\partial z}\frac{1}{z} - \bar{C}_{22}\frac{1}{z^2} - \bar{C}_{44}\frac{1}{z^2}\beta_m^2\right] + \frac{\partial \bar{C}_{33}}{\partial z}\frac{\partial}{\partial z} + \bar{C}_{33}\frac{\partial^2}{\partial z^2} + \bar{C}_{33}\frac{1}{z}\frac{\partial}{\partial z} + \bar{C}_{55}\frac{\partial^2}{\partial x^2},$$

$$A_{1\theta} = \left[\bar{C}_{44}\frac{1}{z^2}\beta_m - \frac{\partial \bar{C}_{23}}{\partial z}\frac{1}{z}\beta_m + \bar{C}_{22}\frac{1}{z^2}\beta_m\right] - \left[\bar{C}_{23}\frac{1}{z}\beta_m + \bar{C}_{44}\frac{1}{z}\beta_m\right]\frac{\partial}{\partial z},$$

$$A_{1x} = \left[\bar{C}_{55} + \bar{C}_{13}\right]\frac{\partial^2}{\partial z \partial x} + \frac{\partial \bar{C}_{13}}{\partial z}\frac{\partial}{\partial x} + \left[\bar{C}_{13} - \bar{C}_{12}\right]\frac{1}{z}\frac{\partial}{\partial x},$$

$$A_{2z} = \left[\bar{C}_{44}\frac{1}{z^2} + \frac{\partial \bar{C}_{44}}{\partial z}\frac{1}{z} + \bar{C}_{22}\frac{1}{z^2}\right]\beta_m + \left[\bar{C}_{23} + \bar{C}_{44}\right]\frac{1}{z}\beta_m\frac{\partial}{\partial z},$$

$$A_{2\theta} = -\left[\frac{\partial \bar{C}_{44}}{\partial z}\frac{1}{z} + \bar{C}_{44}\frac{1}{z^2} + \bar{C}_{22}\frac{1}{z^2}\beta_m^2\right] + \left[\frac{\partial \bar{C}_{44}}{\partial z} + \bar{C}_{44}\frac{1}{z}\right]\frac{\partial}{\partial z} + \bar{C}_{44}\frac{\partial^2}{\partial z^2} + \bar{C}_{66}\frac{\partial^2}{\partial x^2},$$

$$A_{2x} = \left[\bar{C}_{66} + \bar{C}_{12}\right]\frac{1}{z}\beta_m\frac{\partial}{\partial x},$$

$$A_{3z} = \left[\bar{C}_{55}\frac{1}{z} + \bar{C}_{12}\frac{1}{z} + \frac{\partial \bar{C}_{55}}{\partial z}\right]\frac{\partial}{\partial x} + \left[\bar{C}_{13} + \bar{C}_{55}\right]\frac{\partial^2}{\partial z \partial x},$$

$$A_{3\theta} = -\left[\bar{C}_{12} + \bar{C}_{66}\right]\frac{1}{z}\beta_m\frac{\partial}{\partial x},$$

$$A_{3x} = -\bar{C}_{66}\frac{1}{z^2}\beta_m^2 + \bar{C}_{11}\frac{\partial^2}{\partial x^2} + \bar{C}_{55}\frac{\partial^2}{\partial z^2} + \left[\bar{C}_{55}\frac{1}{z} + \frac{\partial \bar{C}_{55}}{\partial z}\right]\frac{\partial}{\partial z}.$$

References

1. Woo, J., Meguid, S.A.: Nonlinear analysis of functionally graded plates and shallow shells. Int. J. Solids Struct. **38**, 7409–7421 (2001)
2. Loy, C.T., Lam, K.Y., Reddy, J.N.: Vibration of functionally graded cylindrical shells. Int. J. Mech. Sci. **41**, 309–324 (1999)
3. Pradhan, S.C., Loy, C.T., Lam, K.Y., Reddy, J.N.: Vibration characteristics of functionally graded cylindrical shells under various boundary conditions. Appl. Acoust. **61**, 111–129 (2000)
4. Chen, W.Q., Kang Yong, L., Ding, H.J.: On free vibration of non-homogeneous transversely isotropic magneto-electro-elastic plates. J. Sound Vib. **279**, 237–251 (2005)
5. Xiao-Lin, H., Hui-Shen, S.: Vibration and dynamic response of functionally graded plates with piezoelectric actuators in thermal environments. J. Sound Vib. **289**, 25–53 (2006)
6. Sobhani Aragh, B., Yas, M.H.: Three dimensional free vibration of functionally graded fiber orientation and volume fraction of cylindrical panels. Mater. Des. **31**, 4543–4552 (2010)
7. Zhao, X., Lee, Y.Y., Liew, K.M.: Thermoelastic and vibration analysis of functionally graded cylindrical shells. Int. J. Mech. Sci. **51**, 694–707 (2009)
8. Sobhani Aragh, B., Yas, M.H.: Static and free vibration analyses of continuously graded fiber-reinforced cylindrical shells using generalized power-law distribution. Acta Mech. **215**, 155–173 (2010)
9. Sobhani Aragh, B., Yas, M.H.: Effect of continuously grading fiber orientation face sheets on vibration of sandwich panels with FGM core. Int. J. Mech. Sci. **53**, 628–638 (2011)
10. Columbia Accident Investigation Board: Report of Columbia accident investigation board, vol. I, chap 6 (PDF). p. 173 (2003)
11. Columbia Accident Investigation Board: In-flight options assessment, vol. II, appendix D.12 (PDF). 30 January 2006 (2003)
12. Goupee, A.J., Vel, S.S.: Two-dimensional optimization of material composition of functionally graded materials using meshless analyses and a genetic algorithm. Comput. Methods Appl. Mech. Eng. **195**, 5926–5948 (2006)
13. Nemat-Alla, M.: Reduction of thermal stresses by developing two-dimensional functionally graded materials. Int. J. Solids Struct. **40**, 7339–7356 (2003)
14. Hedia, H.S.: Comparison of one-dimensional and two-dimensional functionally graded materials for the backing shell of the cemented acetabular cup. J. Biomed. Mater. Res. Part B Appl. Biomater. **74**, 732–739 (2005)
15. Hedia, H.S., Shabara, M.A.N., El-Midany, T.T. et al.: Improved design of cementless hip stems using two-dimensional functionally graded materials. J. Biomed. Mater. Res. Part B Appl. Biomater. **79**, 42–49 (2006)
16. Sutradhar, A., Paulino, G.H.: The simple boundary element method for transient heat conduction in functionally graded materials. Comput. Methods Appl. Mech. Eng. **193**, 4511–4539 (2004)
17. Chan, Y.S., Gray, L.J., Kaplan, T. et al.: Green's function for a two-dimensional exponentially graded elastic medium. Proc. R. Soc. Lond. Ser. A **460**, 1689–1706 (2004)
18. Qian, L.F., Batra, R.C.: Design of bidirectional functionally graded plate for optimal natural frequencies. J. Sound Vib. **280**, 415–424 (2005)
19. Asgari, M., Akhlaghi, M., Hosseini, S.M.: Dynamic analysis of two-dimensional functionally graded thick hollow cylinder with finite length under impact loading. Acta Mech. **208**, 163–180 (2009)
20. Asgari, M., Akhlaghi, M.: Transient thermal stresses in two-dimensional functionally graded thick hollow cylinder with finite length. Arch. Appl. Mech. **80**, 353–376 (2010)
21. Nemat-Alla, M., Ahmed, A.I.E., Hassab-Allah, I.: Elastic–plastic analysis of two-dimensional functionally graded materials under thermal loading. Int. J. Solids Struct. **46**, 2774–2786 (2009)
22. Kutiš, V., Murín, J., Belák, R., Paulech, J.: Beam element with spatial variation of material properties for multiphysics analysis of functionally graded materials. Comput. Struct. **89**, 1192–1205 (2011)
23. Goupee, A.J., Vel, S.S.: Two-dimensional optimization of material composition of functionally graded materials using meshless analyses and a genetic algorithm. Comput. Methods Appl. Mech. Eng. **195**, 5926–5948 (2006)
24. Ke, L.L., Wang, Y.S.: Two-dimensional contact mechanics of functionally graded materials with arbitrary spatial variations of material properties. Int. J. Solids Struct. **43**, 5779–5798 (2006)
25. Tornabene, F.: Free vibration analysis of functionally graded conical cylindrical shell and annular plate structures with a four-parameter power-law distribution. Comput. Meth. Appl. Mech. Eng. **198**, 2911–2935 (2009)

26. Viola, E., Tornabene, F.: Free vibrations of three parameter functionally graded parabolic panels of revolution. Mech. Res. Commun. **36**, 587–594 (2009)
27. Tornabene, F., Viola, E.: Free vibration analysis of four-parameter functionally graded parabolic panels and shells of revolution. Eur. J. Mech. A Solid **28**, 991–1013 (2009)
28. Sobhani Aragh, B., Yas, M.H.: Three-dimensional analysis of thermal stresses in four-parameter continuous grading fiber reinforced cylindrical panels. Int. J. Mech. Sci. **52**, 1047–1063 (2010)
29. Vel, S.S., Batra, R.C.: Exact solution for thermoelastic deformations of functionally graded thick rectangular plates. AIAA J. **40**, 1421–1433 (2002)
30. Vel, S.S.: Exact elasticity solution for the vibration of functionally graded anisotropic cylindrical shells. Compos. Struct. **92**, 2712–2727 (2010)
31. Mori, T., Tanaka, K.: Average stress in matrix and average elastic energy of materials with misfitting inclusions. Acta Metall. **21**, 571–574 (1973)
32. Benveniste, Y.: A new approach to the application of Mori–Tanaka's theory of composite materials. Mech. Mater. **6**, 147–157 (1987)
33. Shu, C.: Differential quadrature and its application in engineering. Springer, Berlin (2000)
34. Shu, C., Richards, B.E.: Application of generalized differential quadrature to solve two-dimensional incompressible Navier Stokes equations. Int. J. Numer. Meth. Fluids **15**, 791–798 (1992)
35. Bert, C.W., Malik, M.: Differential quadrature method in computational mechanics, a review. Appl. Mech. Rev. **49**, 1–28 (1996)
36. Matsumaga, H.: Free vibration and stability of functionally graded shallow shells according to a 2-D higher-order deformation theory. J. Compos. Struct. **84**, 132–146 (2008)
37. Farid, M., Zahedinejad, P., Malekzade, H.P.: Three dimensional temperature dependent free vibration analysis of functionally graded material curved panels resting on two parameter elastic foundation using a hybrid semi-analytic, differential quadrature method. Mater. Des. **31**, 2–13 (2010)
38. Pradyumna, S., Bandyopadhyay, J.N.: Free vibration analysis of functionally graded panels using higher-order finite-element formulation. J. Sound Vib. **318**, 176–192 (2008)
39. Varadan, T.K., Bhaskar, K.: Bending of laminated orthotropic cylindrical shells-an elasticity approach. Compos. Struct. **17**, 141–156 (1991)